Geomechanics and Engineering, *Vol. 21, No. 1 (2020) 35-51*
DOI: https://doi.org/10.12989/gae.2020.21.1.035

Seismic response analysis of embankment dams under decomposed earthquakes

Fatemeh Nasiri[a], Hamed Javdanian* and Ali Heidari[b]

Department of Civil Engineering, Shahrekord University, Shahrekord, Iran

(Received December 3, 2019, Revised February 22, 2020, Accepted March 5, 2020)

Abstract. In this study, the seismic response analysis of embankment dams was investigated through numerical modeling. The seismic behavior of dams under main earthquake records and wavelet-based records were studied. Earthquake records were decomposed using de-noising method (DNM) and down-sampling method (DSM) up to five levels. In decomposition process, low and high frequencies of the main earthquake record were separated into two signals. Acceleration response, spectral acceleration, and Fourier amplitude spectrum at the crest of embankment dams under different decomposition levels were evaluated. The seismic behavior under main and decomposed earthquake records was compared. The results indicate an acceptable agreement between the seismic responses of embankment dams under wavelet-based decomposed records and main earthquake motions. Dynamic analyses show that the DNM-based decomposed earthquake records have a better performance compared to DSM-based records. DNM-based records up to level 4 and DSM-based records up to level 2 have a high accuracy in assessment of seismic behavior of embankment dams. The periods corresponding to the maximum values of acceleration spectra and the frequencies corresponding to the maximum values of Fourier amplitude spectra of embankment dam crest under main and decomposed records are in good agreement. The results demonstrate that the main earthquake records can be replaced by wavelet-based decomposed records in seismic analysis of embankment dams.

Keywords: embankment dam; earthquake; seismic response; wavelet; numerical modeling

1. Introduction

It is essential to evaluate dynamic behavior of embankment dams under seismic loading. Various methods have been used for dynamic analysis of embankment dams (e.g., Uddin 1999, Hwang *et al.* 2007, Papadimitriou *et al.* 2014, Terzi and Selcuk 2015, Russo *et al.* 2017, Nasiri *et al.* 2019, Chakraborty *et al.* 2019, Hu and Huang 2019). Elgamal *et al.* (1990) analyzed dynamic behavior of the La Villita embankment dam by sliding block analysis method. Papalou and Bielak (2001, 2004) analyzed the seismic response of the La Villita dam by finite element method (FEM).

Pelecanos and co-workers studied effects of dam-reservoir interactions and valley geometry on the seismic response of the La Villita embankment dam (Pelecanos *et al.* 2015, 2018). Through FEM and displacement-based analyses, Rampello *et al.* (2009) investigated the seismic behavior of the Marana Capacciotti embankment dam (Cascone and Rampello 2003). They found a decrease in seismic displacements and maximum acceleration of the crest of embankment dam with increasing bedrock depth. Ding *et al.* (2013) and Aliberti *et al.* (2016) numerically studied the seismic response of Shiziping and San Pietro dams, respectively.

Castelli *et al.* (2016) compared maximum horizontal accelerations obtained from dynamic analysis of the Lentini embankment dam under Santa Lucia Earthquake by different numerical methods. The failure mechanisms and dynamic behavior of the Fujinuma embankment dam failed under Pacific Coast of Tohoku Earthquake were studied by Charatpangoon *et al.* (2014). Some researchers studied the earthquake-induced behavior of embankment dams through physical modeling of shaking table (Wang *et al.* 2017) and centrifuge experiments (Park and Kim 2017).

The seismic response of concrete faced rockfill dams (CFRDs) has been analyzed under earthquake-induced vibrations (Bayraktar and Kartal 2010, Zou *et al.* 2013, Chen *et al.* 2016, Karabulut and Genis 2019). The dynamic behavior of this type of dams was evaluated under non-uniform seismic loading by FEM (Yao *et al.* 2019). Xu *et al.* (2015) analyzed the dynamic behavior of concrete faced rockfill dams and found that acceleration and seismic deformations of CFRDs are affected by rockfill characteristics, and concrete shell does not significantly influence the seismic behavior.

Feng *et al.* (2010) evaluated the seismic response of the Liyutan embankment dam under Chi-Chi Earthquake. According to numerical results of Andrianopoulos *et al.* (2014) on the seismic behavior of embankment dams, the maximum acceleration of dam crest is influenced by input motion characteristics, dam height and stiffness of foundation soil. The effect of near-field and far-field earthquakes on nonlinear response of embankment dams has also been investigated (Davoodi *et al.* 2013a). Some

*Corresponding author, Assistant Professor
E-mail: javdanian@sku.ac.ir
[a]M.Sc. Student
[b]Associate Professor

ISSN: 2005-307X (Print), 2092-6219 (Online)

researchers investigated seismic deformations and settlements of embankment dams and developed models to evaluate the earthquake-induced behavior of these structures (Jafarian *et al.* 2015, Javdanian *et al.* 2018, 2020, Lashgari *et al.* 2018, Javdanian and Pradhan 2019, Shakarami *et al.* 2019). Through modeling the Masjed Soleyman dam by FLAC finite difference method, Davoodi et al. (2013b) investigated the effect of spatial variation of earthquake ground motion (SVEGM) (Apaydin *et al.* 2016, Bas *et al.* 2018) on the seismic behavior of embankment dams. According to the results, SVEGM affects the seismic response of embankment dams which is consistent with the numerical results of Chen and Harichandran (2001) on the Santa Felicia embankment dam. Sharafi and Maleki (2019) studied the effect of near-fault earthquakes on the seismic response of embankment dams. Their results indicate that the linear response analysis leads to a greater response than nonlinear method (Sonmezer *et al.* 2018, 2019, Sonmezer and Celiker 2020). All studies on the seismic response analysis of embankment dams focus on main earthquake records with a wide range of frequencies. Wavelet transform (WT) is one of the best methods for separating earthquake frequencies (e.g., Banjade *et al.* 2019).

Wavelet transform (WT) is a powerful tool for signal analysis capable of providing earthquake records simultaneously in both time and frequency domains (Kaveh and Mahdavi 2016). This method has been widely used for seiamic analysis including dynamic behavior of geomaterials (Haigh *et al.* 2002), dynamic analysis of structures (Salajegheh *et al.* 2005), filtering ground motion records (Ansari et al. 2007, Ghodrati Amiri *et al.* 2014), and synthetic record generation (Suarez and Montejo 2007). This method has also been used for optimal design of structures under earthquake loading (Salajegheh and Heidari 2005a, b). According to To *et al.* (2009), wavelet transform outperforms Fourier transform in correcting geophysical data.

Review of the available technical literature indicates that wavelet transform is a powerful technique for correcting and decomposing earthquake motion records. A question arises, “Is it possible to replace main earthquake records with wavelet-based decomposed records in practical problems of geotechnical earthquake engineering such as seismic response analysis of embankment dams?”. This study focuses on the seismic response analysis of embankment dams under main and wavelet-based decomposed earthquake shakings. Seismic analyses of short and high embankment dams were conducted through finite element numerical modeling of Plaxis program. Earthquake records were decomposed using de-noising and down-sampling methods up to 5 levels. Seismic responses at the crest of embankment dams under various decomposition levels of records were investigated. Horizontal acceleration response, spectral acceleration, and Fourier amplitude spectrum under main and decomposed earthquake motions were studied and compared. The performance of decomposed records in assessment of seismic response analysis of embankment dams was explored.

2. Wavelet transform

Wavelet transform (WT) is utilized as an advanced mathematical tool for signal processing. Wavelet theory has been used in different civil engineering problems (e.g., Salajegheh and Heidari 2005a, b, Moghaddam and Bagheripour 2014, Smyrou *et al.* 2016). To better understand of performance of the wavelet transform, it can be compared with Fourier transform. Regardless of the position of frequency occurrence, Fourier transform decomposes a signal as different exponents of sinusoidal waves and frequency. Unlike the Fourier transform, wavelet transform operates proportional to frequency (Daubechies 1990, Rioul and Vetterli 1991, Farge 1992). Wavelet scale decreases by increasing frequency along the time series and vice versa (Heidari *et al.* 2019). Wavelet transforms include continuous and discrete transforms. In continuous wavelet transform (CWT), the considered expanded or contracted frame is transformed, then time integral is taken after multiplying it by the signal. CWT is defined as follows:

$$CWT_r^{\rho} = \int r(t)\rho_{a,b}^{*}(t)dt \tag{1}$$

where $r(t)$ is the main wave (i.e., acceleration time history in the current research), a is the scale corresponding to the inverse of frequency, b represents transformation, the index * shows complex conjugate pair, and $\boldsymbol{\rho}$ is the main wave function to generate other functions. All $\rho_{a,b}^{*}$ functions derived from the main function are called wavelet functions and obtained from the following equation:

$$\rho_{a,b}(t) = \frac{1}{\sqrt{a}}\rho\left(\frac{t-b}{a}\right) \tag{2}$$

Discrete wavelet transform (DWT) is a wavelet series which is attained from continuous wavelet transform (CWT) (Crochiere 1981). In this approach, a type of time-scale description of the discrete signal is presented by digital filters. Filters with different cutoff frequencies are utilized in DWT for signal analysis with various scales. Different frequencies of a signal are analyzed by passing it through low- and high-pass filters. In this method, the signal resolution is controlled by the performance of filters and the scale varies through up/down-sampling techniques (Salajegheh *et al.* 2005). The discrete values of $b = ka_0^j b_0$ and $a = a_0^j$ are substituted in Eq. (2) to calculate the DWT coefficients:

$$\rho_{j,k}(t) = \frac{1}{\sqrt{a_0^j}}\rho\left(\frac{t-ka_0^j b_0}{a_0^j}\right) \tag{3}$$

Simplifying the Eq. (3) yields:

$$\rho_{j,k}(t) = a_0^{\frac{-j}{2}}\rho\left(a_0^{-j}t - kb_0\right) \tag{4}$$

By substituting Eq. (4) in Eq. (1), DWT is (Eq. 5):

$$DWT_r^{\rho} = \int_{-\infty}^{+\infty} r(t)\rho_{j,k}^{*}(t)dt \tag{5}$$

It should be noted that in CWT method, all possible frequencies or scales of time series are identified and analyzed while a limited number of scales are analyzed in

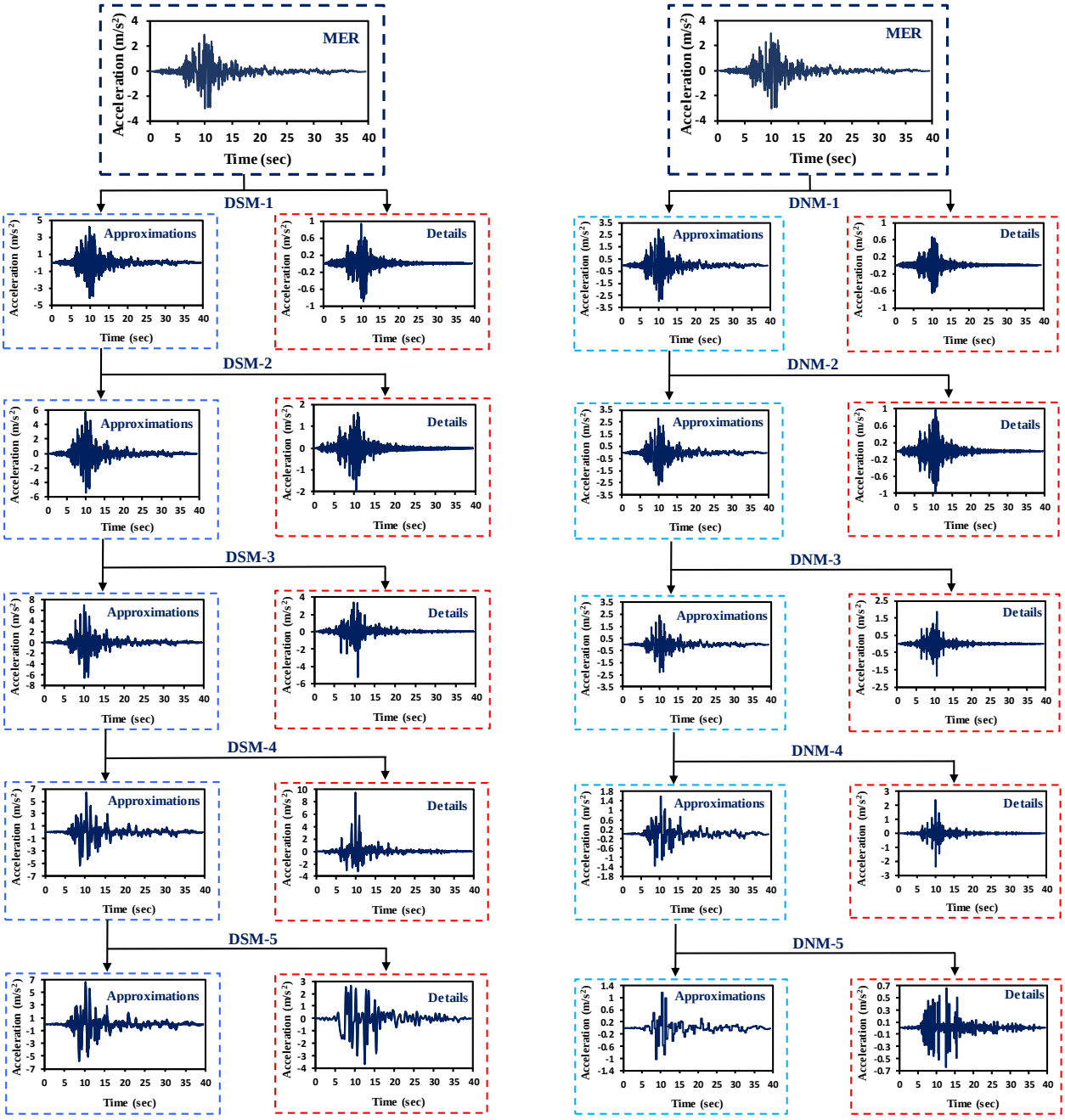

Fig. 1 DNM and DSM-based decomposition processes of Imperial Valley earthquake record

the DWT method (Rioul and Vetterli 1991).

2.1 Wavelet de-noising

In the de-noising method (DNM), the main earthquake wave is divided into low and high frequencies without down-sampling. The low and high frequencies are obtained from the functions r and **ρ** respectively. The low and high frequency components of the earthquake are, respectively, called approximations and details. High frequencies of the earthquake record are omitted in the discrete wavelet transform (DWT) method. Another wavelet transform is applied on low earthquake record frequencies to divide them into approximation and details, after which the latter are eliminated. This process is repeated until high earthquake frequencies are eliminated and the error between the resulting earthquake and the main earthquake wave is sufficiently small (e.g., Ansari *et al.* 2010). Decomposition processes of Imperial Valley earthquake record based on de-noising method (DNM) is shown in Fig. 1.

2.2 Wavelet down-sampling

In the down-sampling method (DSM), the signal first passes through a sub-band low-pass digital filter and all frequency larger than half of the largest frequency are eliminated. Due to the largest frequency in the signal exiting in the filter equals to $\pi/2$ radians, half of the samples can be omitted (Holschneider 1995).

Due to the largest frequency in the signal exiting in the

filter equals to $\pi/2$ radians, half of the samples can be omitted (Holschneider 1995). By alternate elimination of the samples, the signal length is halved without elimination of the record information. A similar process is carried out by a sub-band high-pass digital filter. Consequently, the length of the low-pass (approximations) and high-pass (details) outputs of the first step of wavelet transform is half the length of the initial signal. The time resolution is halved while the frequency resolution is doubled in this way. This process can be repeated on low-pass with time resolutions equal to half of before step (e.g., Strang and Nguyen 1996). Details are reduced by increasing the number of transformation steps. This continues as long as there is a slight difference between the resulting approximation wave and the main earthquake wave. DSM-based decomposition processes of Imperial Valley earthquake record is depicted in Fig. 1.

3. Earthquake records

In this study, a total of 16 earthquake records with various magnitudes were used. Table 1 presents the name, station code, date of occurrence, magnitude (M_w), and peak ground acceleration (a_{max}) of the earthquake records. These records were occurred from 1961 to 2004. As presented in Table 1, the earthquakes magnitudes were varied from 4.2 to 7.6. The minimum and maximum a_{max} of the earthquake records used in this study were 0.28 and 3.45 m/s^2, respectively (Table 1). The earthquake records were decomposed using wavelet de-noising and wavelet down-sampling methods up to 5 levels. Each decomposition level is obtained from decomposition of the previous level. For example, the second level was achieved from decomposition of the first level and this process continues to the fifth level.

Table 1 Earthquake records data

No.	Earthquake	Station code	Year	M_w	a_{max} (m/s^2)
1	Abhar	ABH	2002	6.4	0.28
2	Floor East Wall	USGS-13620	1992	7.3	0.68
3	Golbaf	GBF1	1981	6.6	2.04
4	Hollister	USGS-1028	1961	5.5	1.99
5	Imperial Valley	USGS-5115	1979	6.5	3.00
6	Kobe	CUE90	1995	6.9	3.45
7	Kocaeli	KOERI330	1999	7.6	3.23
8	Loma Prieta	CDMG-47381	1989	6.9	3.44
9	Marak	MRK	1997	6.9	0.57
10	Morgan Hill	USGS-47125	1984	6.2	1.34
11	Noshahr	NSH	2004	4.2	0.54
12	Qahrvard	GRD	2002	6.4	0.42
13	Razjerd	RSJ	2004	6.4	0.34
14	Rudsar	RUS	2004	6.4	0.40
15	San Fernando	USGS-15910	1971	6.6	0.92
16	Sarab	SBR	1997	6.0	0.38

Therefore, 16 main earthquake records and 160 decomposed earthquake records (total of 176 records) were used as input motions in dynamic analysis of embankment dams.

4. Numerical modeling

The finite element program of Plaxis (Brinkgreve 2002) was used to assess dynamic behavior of embankment dams under earthquake-induced loading. Numerical methods have been extensively used to evaluate dynamic behavior of embankment dams and soil deposits (e.g., Rampello *et al.* 2009, Ebrahimian 2011, Amorosi *et al.* 2016, Shakarami *et al.* 2019). In this study, seismic response analysis of embankment dams with the height of 50 m and 150 m and the slopes of 1(V):2.2(H) and 1(V):1.5(H), respectively, were evaluated through numerical modeling. The seismic response of embankment dam before the first impounding was analyzed numerically. The plane strain condition with 15-node triangular elements and 12 stress points were utilized for seismic analysis of embankment dams. The geometrical configuration of the embankment dam with clay core in Plaxis modeling is depicted in Fig. 2. The characteristics of the shell, core and foundation materials used in numerical modeling of dams including unit weight (γ), cohesion (C), internal friction angle (φ), permeability (k), elastic modulus (E), and Poisson ratio (υ) are presented in Table 2. In this research, the Mohr–Coulomb elasto-plastic model and elastic model were used to simulate the dam body and dam foundation, respectively.

In static analysis, the bottom of the model was restrained in both vertical and horizontal directions, while vertical boundaries were restrained horizontally. In dynamic analysis, to avoid the influences of wave reflection, absorbent boundaries were used along the horizontal and vertical edges of the finite element modeling. Rayleigh damping was used for seismic analysis of embankment dams. The coefficients of Rayleigh damping were considered as $\alpha=\beta=0.01$. These coefficients were calculated using the relationship $[C]=\alpha[M]+\beta[K]$, where, C, M, and K, are damping, mass, and stiffness matrices, respectively (Brinkgreve 2002).

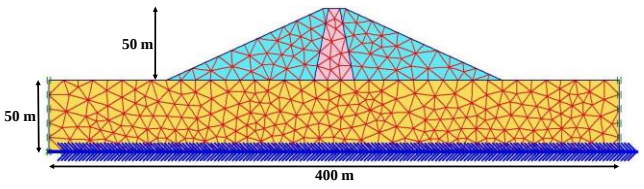

Fig. 2 Geometrical configuration of numerical modeling of embankment dam

Table 2 Dam characteristics in numerical analysis

Material	γ (kN/m^3)	C (kPa)	φ (deg.)	E (MPa)	k (cm/s)	υ (-)
Core	17.5	30	25	27	10^{-7}	0.30
Shell	20	20	30	31	2×10^{-3}	0.25
Foundation	20	-	-	1000	10^{-6}	0.25

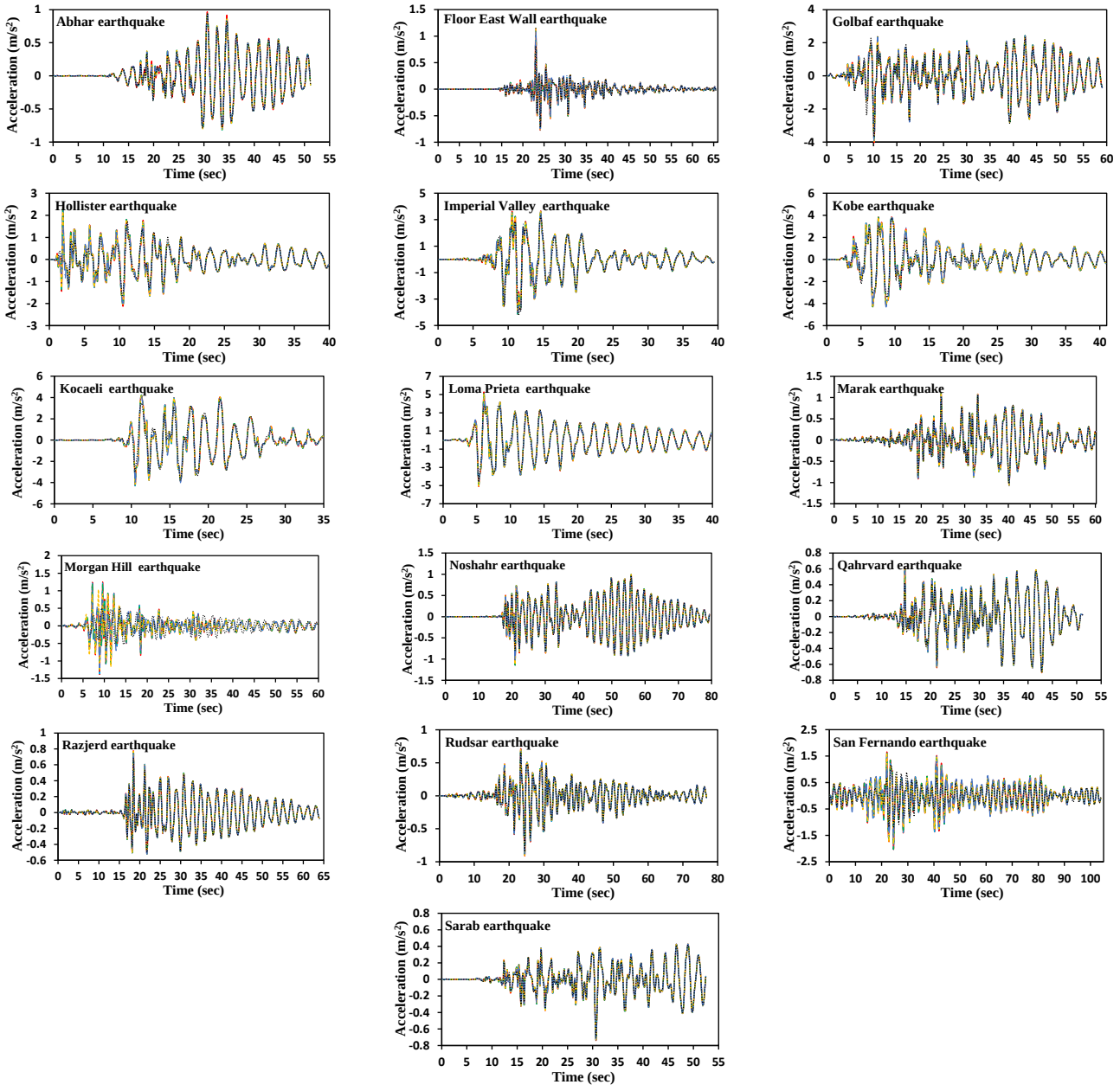

Fig. 3 Acceleration response at the dam crest (H=50 m) under MERs and DNM-based decomposed records

In order to appropriate wave propagation in soil media during dynamic analysis, the dimension of elements (Δl) in the numerical modeling of embankment dam was determined based on the Kuhlemeyer and Lysmer (1973)'s criteria as $\Delta l \leq \lambda/10$. The parameter λ ($=V_s/f$) is the wavelength corresponding to the highest frequency of the seismic excitement. This parameter is calculated based on of the minimum shear wave velocity (V_s) and maximum frequency (f) of excitement. The input motion was applied to the dam foundation in form of acceleration time history. Then, the seismic behavior of the crest of embankment dams under various earthquake records were evaluated.

5. Results and discussions

In this section, the results of seismic response analysis of embankment dams with the height of 50 m and 150 m were presented. Acceleration response, spectral acceleration, and Fourier amplitude spectrum (as common criteria for evaluation of seismic behavior of geo-structures) at the crest of embankment dams under main earthquake records (MERs) and wavelet-based decomposed earthquake records (DERs) were discussed.

5.1 Horizontal acceleration response

Embankment dams with a height of 50 and 150 m were dynamically analyzed by finite element method (FEM) under 16 main earthquake records and corresponding decomposed records.

Figs. 3 and 4 respectively compare horizontal accelerations of the crest of the 50 m-high embankment

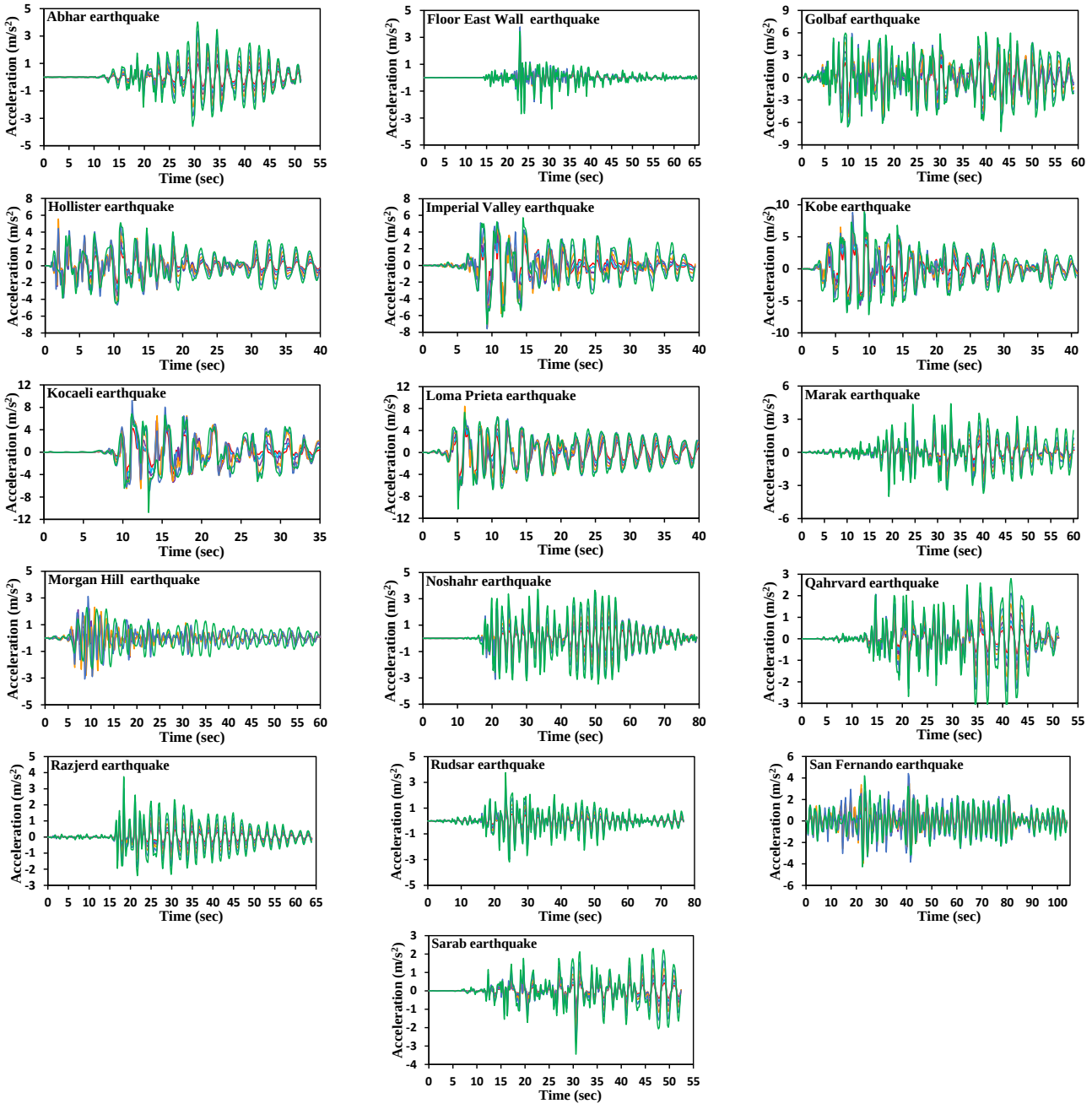

Fig. 4 Acceleration response at the dam crest (H=50 m) under MERs and DSM-based decomposed records

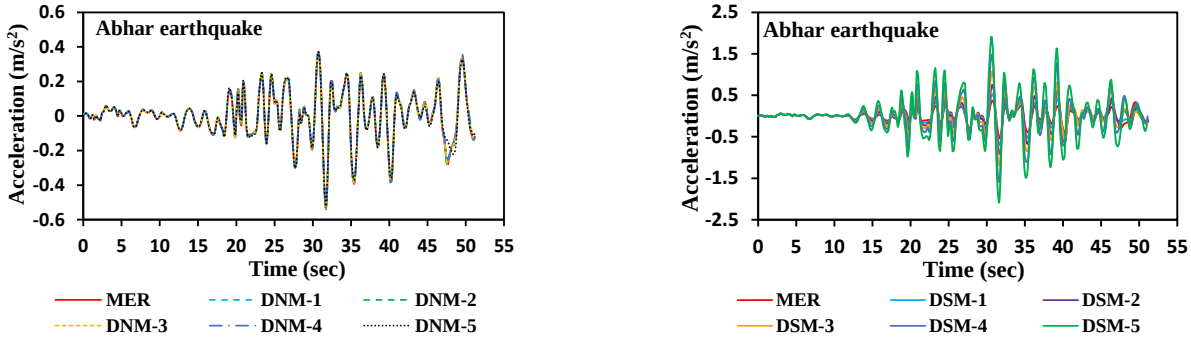

Fig. 5 Acceleration response at the dam crest (H=150 m) under MERs and decomposed records, DNM-based records (left column) and DSM-based records (right column)

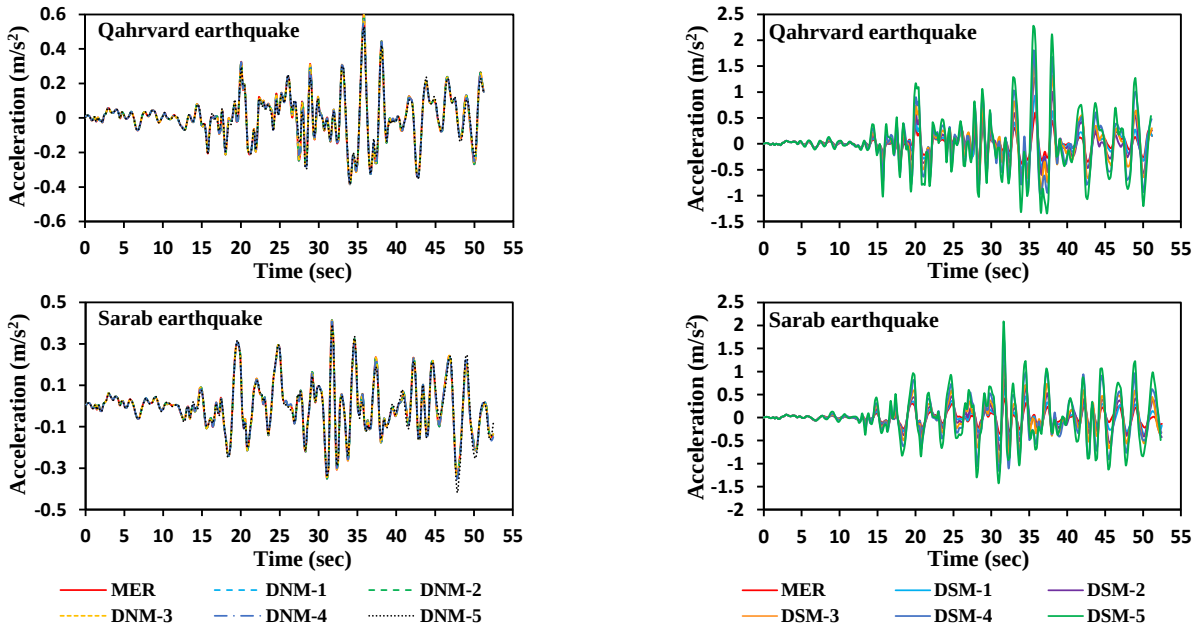

Fig. 5 Continued

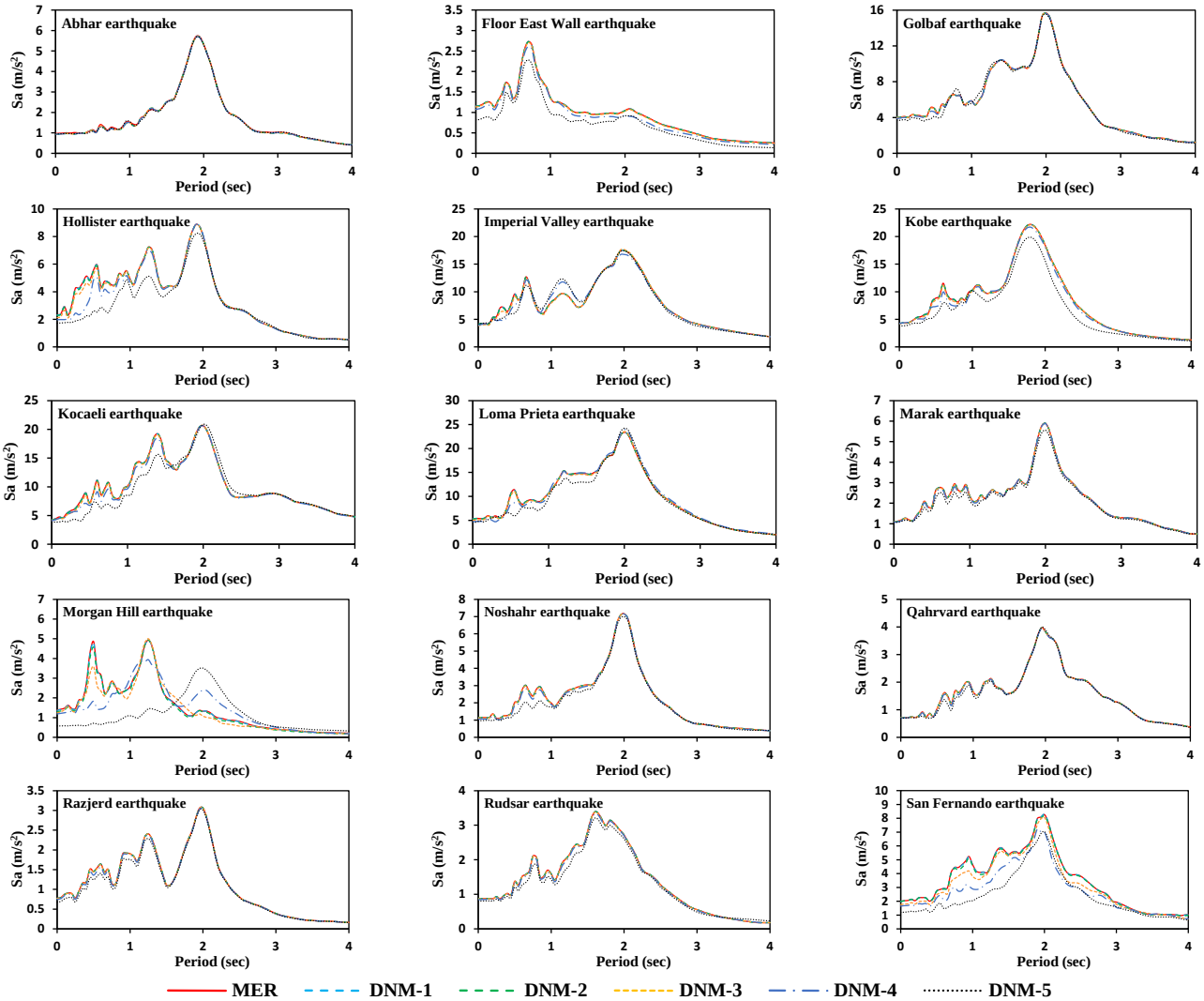

Fig. 6 Spectral acceleration response at the dam crest (H=50 m) under MERs and DNM-based decomposed records

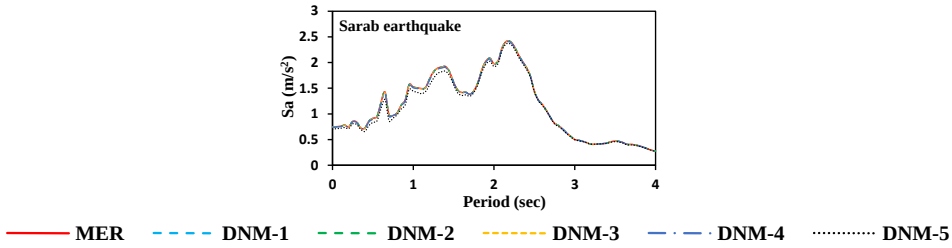

Fig. 6 Continued

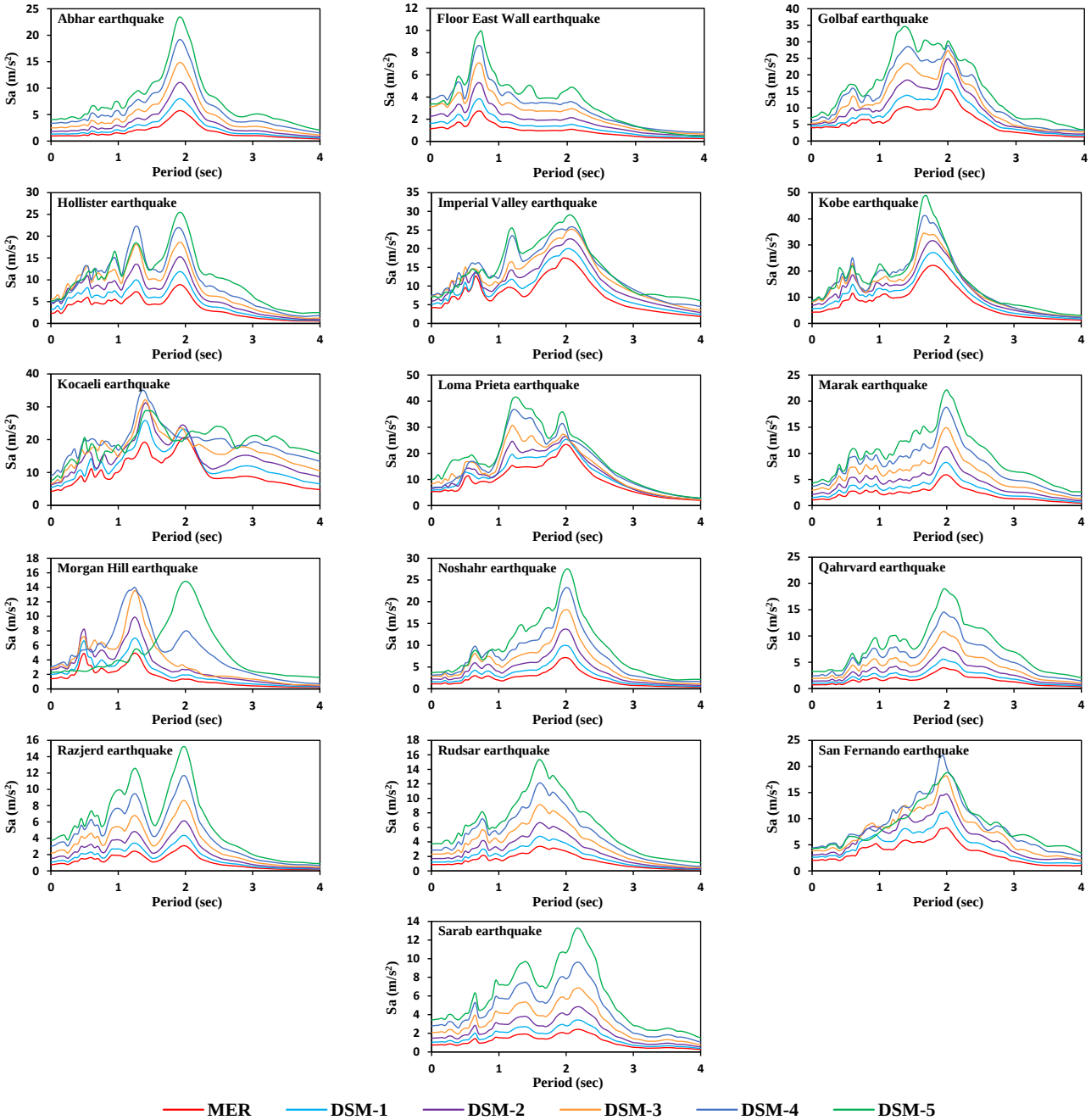

Fig. 7 Spectral acceleration response at the dam crest (H=50 m) under MERs and DSM-based decomposed records

dam under main earthquake records and wavelet-based decomposed earthquake records by de-noising and down-sampling methods. Dynamic analyses were carried out under decomposed records up to five levels (i.e., DNM-1 to DNM-5 and DSM-1 to DSM-5). Fig. 5 compares accelerations of the crest of the 150-m high embankment dam under three main earthquake records and DNM- and DSM-based decomposed earthquake records. The results

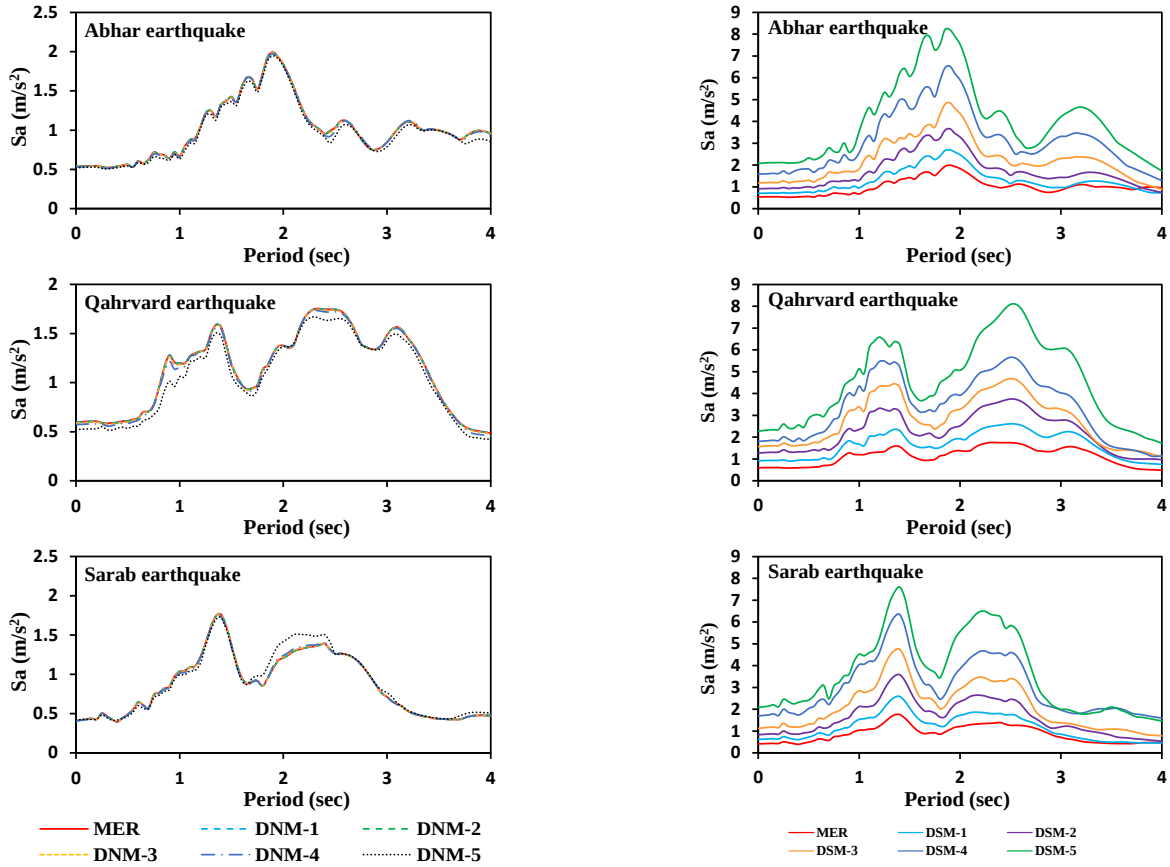

Fig. 8 Spectral acceleration response at the dam crest (H=150 m) under MERs and decomposed records, DNM-based records (left column) and DSM-based records (right column)

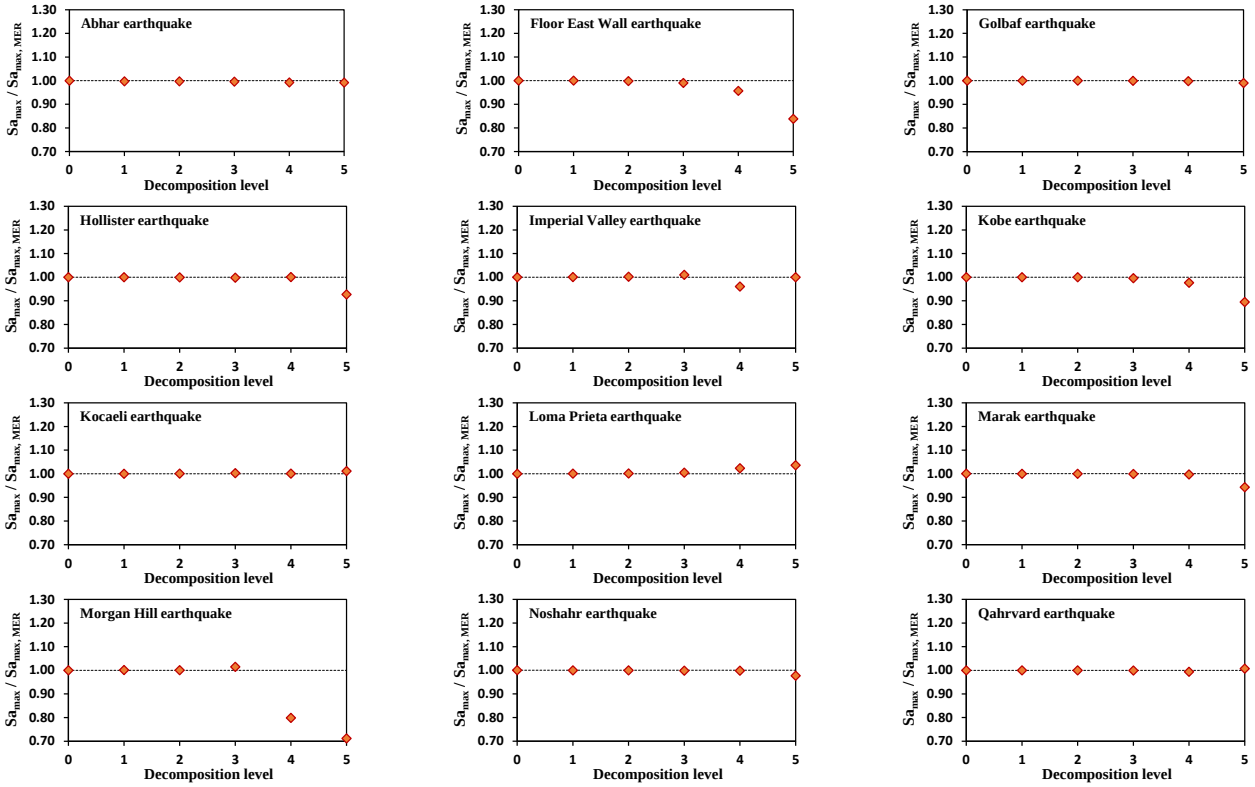

Fig. 9 The ratio of maximum acceleration spectrum at the dam crest (H=50 m) under MERs and DNM-based decomposed records

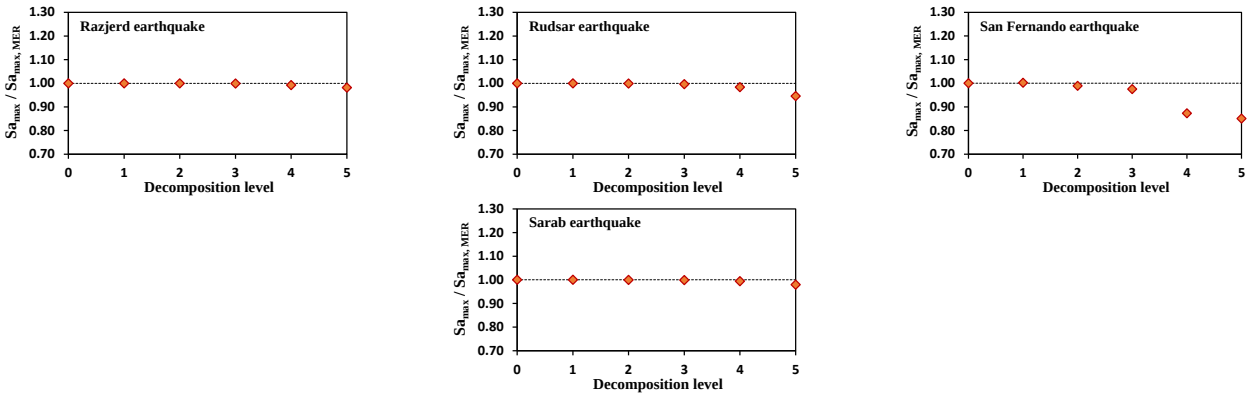

Fig. 9 Continued

Table 3 Accuracy of spectral acceleration response at the dam crest (H=50 m) under decomposed records

Earthquake	RMSE									
	DNM-1	DNM-2	DNM-3	DNM-4	DNM-5	DSM-1	DSM-2	DSM-3	DSM-4	DSM-5
Abhar	0.03068	0.03062	0.03063	0.03315	0.03993	0.8564	2.0246	3.5197	5.2771	7.0443
Floor East Wall	0.0007	0.0036	0.0149	0.0822	0.2352	0.4472	1.0535	1.8315	2.4956	3.0525
Golbaf	0.0010	0.0051	0.0215	0.09812	0.3371	2.1351	4.4726	6.75	9.2577	12.1982
Hollister	0.0069	0.0344	0.1422	0.5494	1.1083	1.5078	3.358	5.2712	6.9397	7.8731
Imperial Valley	0.0075	0.0333	0.1794	0.7793	0.9595	1.7083	3.5148	5.2538	6.7303	7.7299
Kobe	0.0056	0.0263	0.1327	0.5307	1.7327	2.414	4.6935	6.4255	8.4608	9.8160
Kocaeli	0.0080	0.0396	0.1505	0.5304	1.6231	2.7582	5.3411	7.4648	9.8016	10.021
Loma Prieta	0.0074	0.0349	0.1415	0.5836	1.1889	2.0392	3.5784	5.7656	8.4313	10.7202
Marak	0.0006	0.0028	0.0117	0.0438	0.1694	1.0185	2.3723	4.1211	6.1496	8.1692
Morgan Hill	0.0180	0.0862	0.289	0.7057	1.5043	0.8037	1.8614	2.9529	4.3267	5.1495
Noshahr	0.0008	0.0042	0.0174	0.0739	0.2974	1.1223	2.6322	4.4903	6.6065	8.8144
Qahrvard	0.0004	0.0017	0.0072	0.0283	0.0846	0.7494	1.8004	3.2274	5.0433	7.2176
Razjerd	0.0003	0.0013	0.0056	0.0277	0.0897	0.5746	1.3867	2.5229	3.9921	5.6242
Rudsar	0.0004	0.0022	0.0093	0.0362	0.1361	0.6787	1.6023	2.806	4.2229	5.6671
San Fernando	0.0141	0.0734	0.3734	0.8846	1.3468	1.4714	3.1549	4.5596	6.0254	5.759
Sarab	0.0003	0.0009	0.0031	0.0127	0.0579	0.5372	1.2923	2.3485	3.7637	5.4314

indicated that acceleration responses under de-noising- and down-sampling-based decomposed earthquake records have a an acceptable accuracy in comparison with those of the embankment dam crest under main earthquake records up to the levels 4 (Figs. 3 and 5) and 2 (Figs. 4 and 5), respectively.

Comparing acceleration responses of the crest of 50 and 150 m high embankment dams under DNM and DSM-based decomposed earthquake records indicates a decrease in the horizontal acceleration of the dam crest with increasing height of the embankment dam (Figs. 3-5). This can be attributed to increase absorption of earthquake energy with increasing dam height. This is in agreement with the results of numerical study of Ebrahimian (2011) who reported that the crest acceleration decreases with increasing the earth dam height.

5.2 Spectral acceleration

Figs. 6 and 7 respectively show spectral acceleration response of the crest of the 50 m high embankment dam under main earthquake records (Table 1) and those decomposed by de-noising and down-sampling methods. The acceleration response spectra were calculated at a damping rate of 5%. As depicted in Fig. 6, the spectral acceleration responses under DNM-based decomposed earthquake records up to level 4 are consistent with the responses under main earthquake records.

Comparing the acceleration response spectra of the embankment dam crest under main earthquakes and DSM-based decomposed earthquake records at five levels indicates a significant difference between responses from the level 2 afterwards (Fig. 7). Similar results were obtained from dynamic analysis of the 150 m high embankment dam under DNM- and DSM-based decomposed earthquake records (Fig. 8). As seen in Figs. 6-8, the periods corresponding to the maximum acceleration spectra (Sa_{max}) of embankment dam crest are consistent under main and wavelet-based decomposed earthquake records.

The root mean square error (RMSE) (Javdanian *et al.*

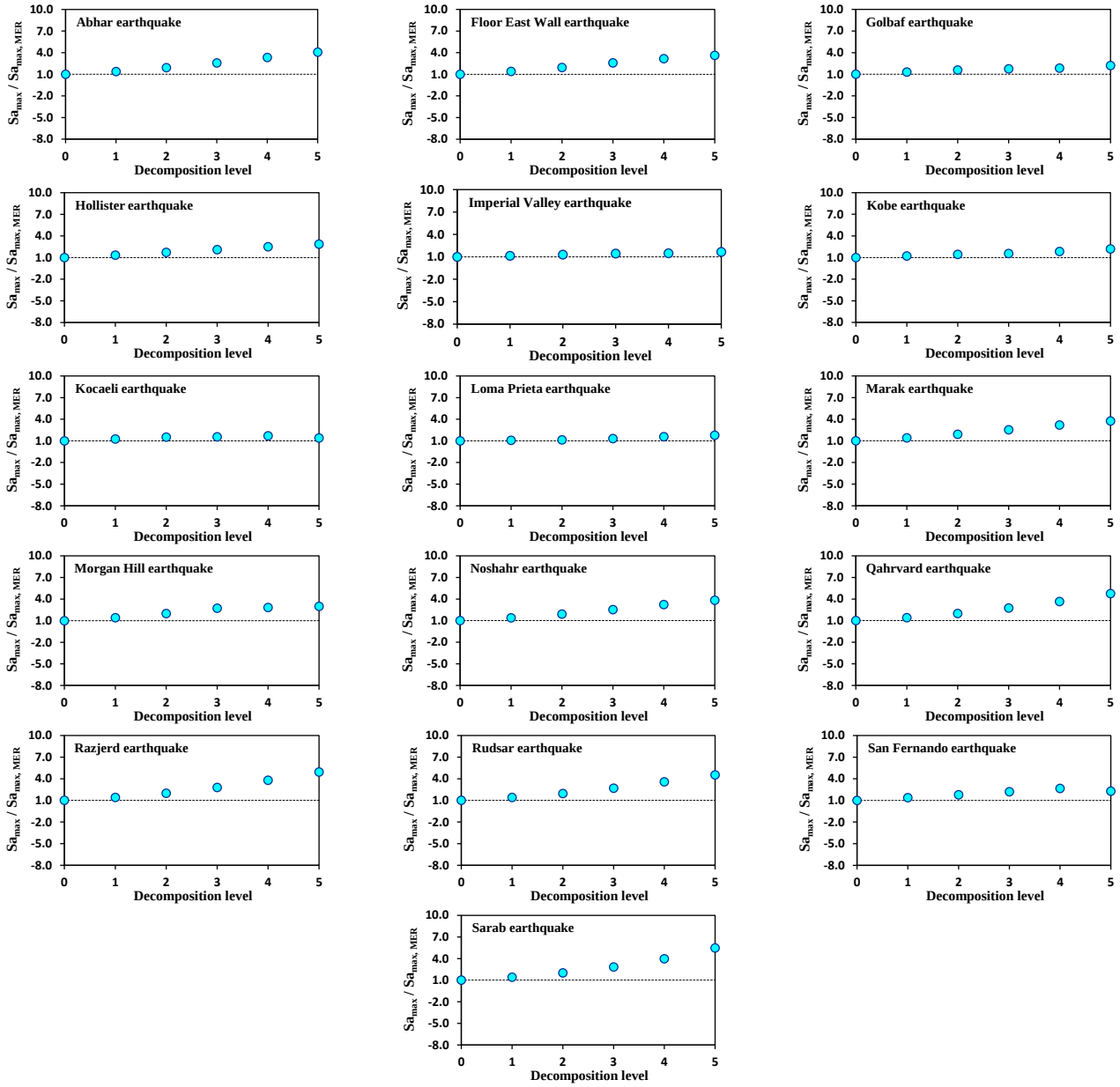

Fig. 10 The ratio of maximum acceleration spectrum at the dam crest (H=50 m) under MERs and DSM-based decomposed records

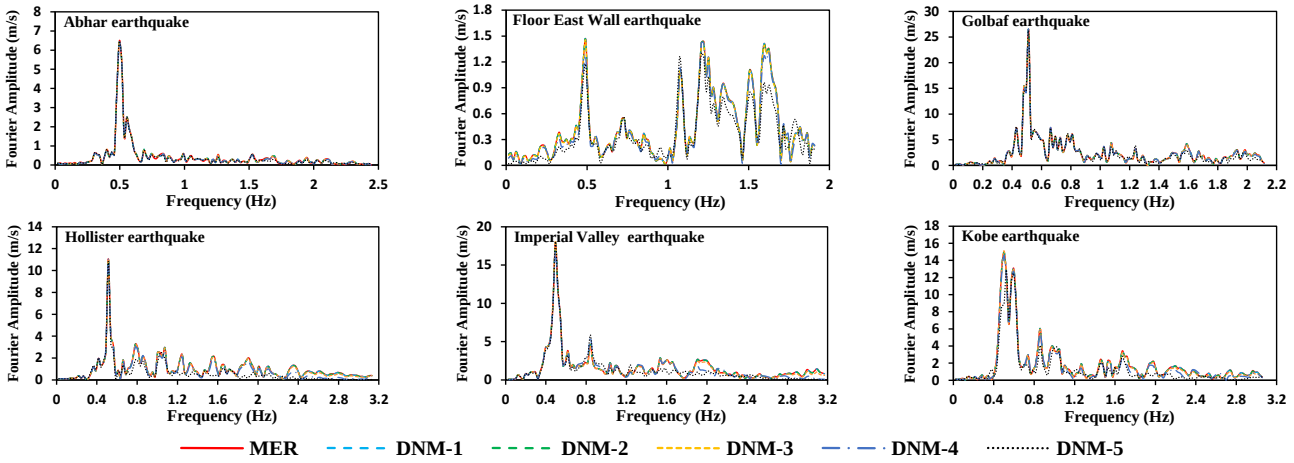

Fig. 11 Fourier amplitude spectrum at the dam crest (H=50 m) under MERs and DNM-based records

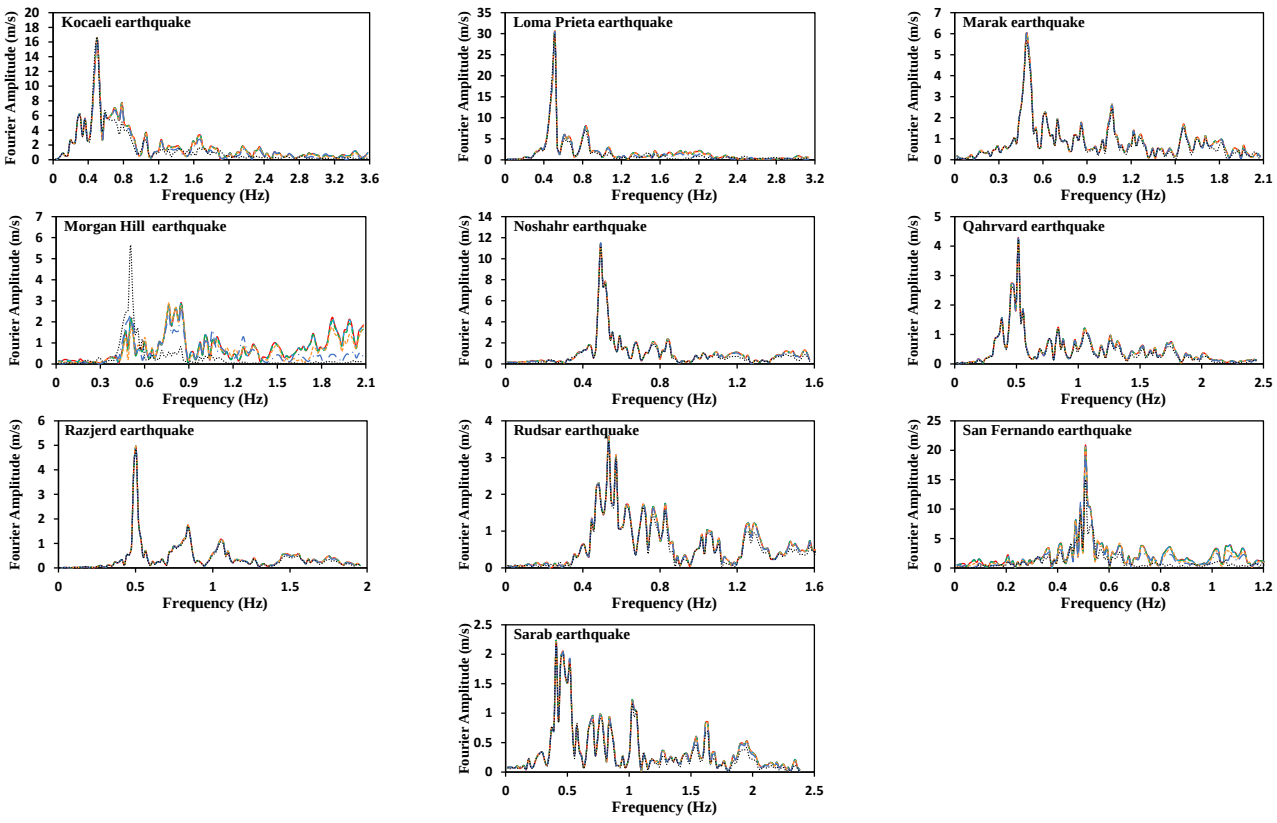

Fig. 11 Continued

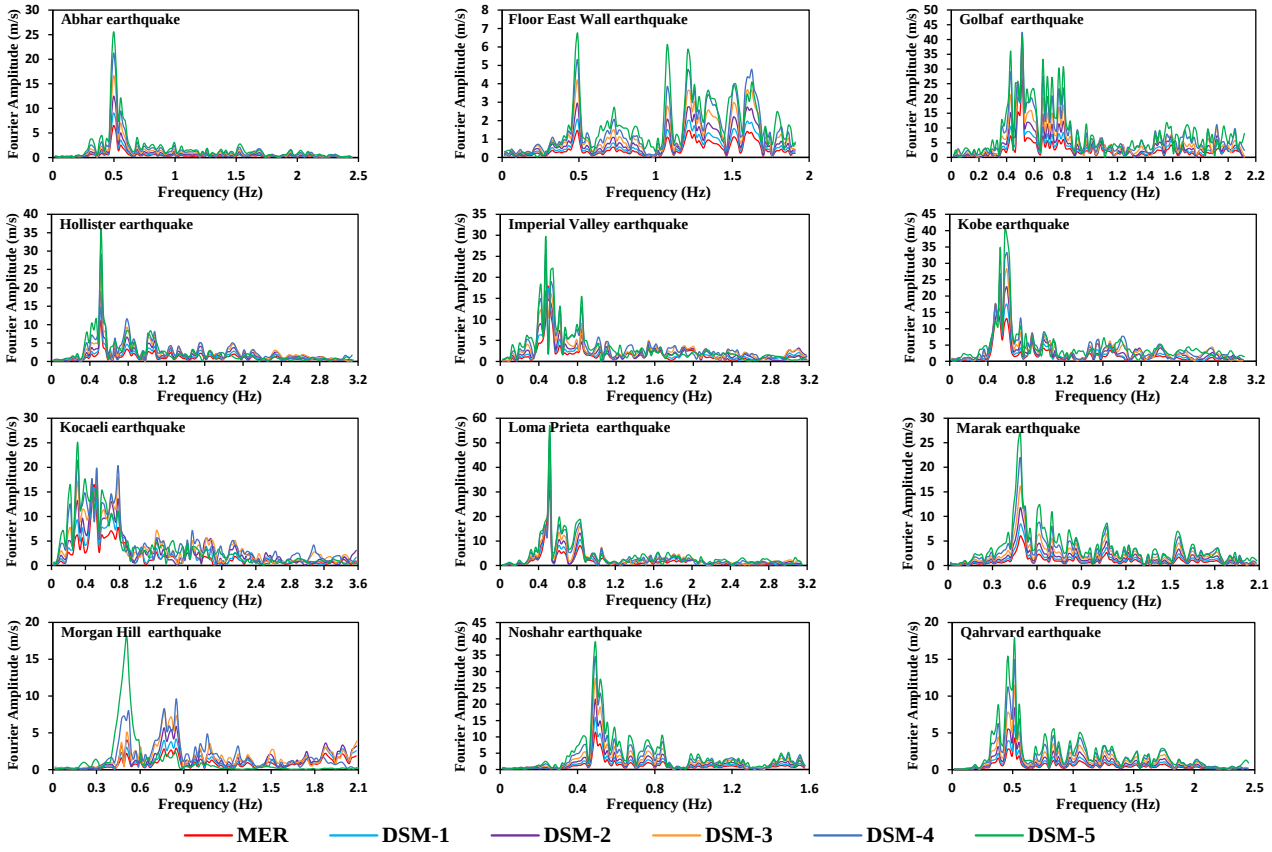

Fig. 12 Fourier amplitude spectrum at the dam crest (H=50 m) under MERs and DSM-based records

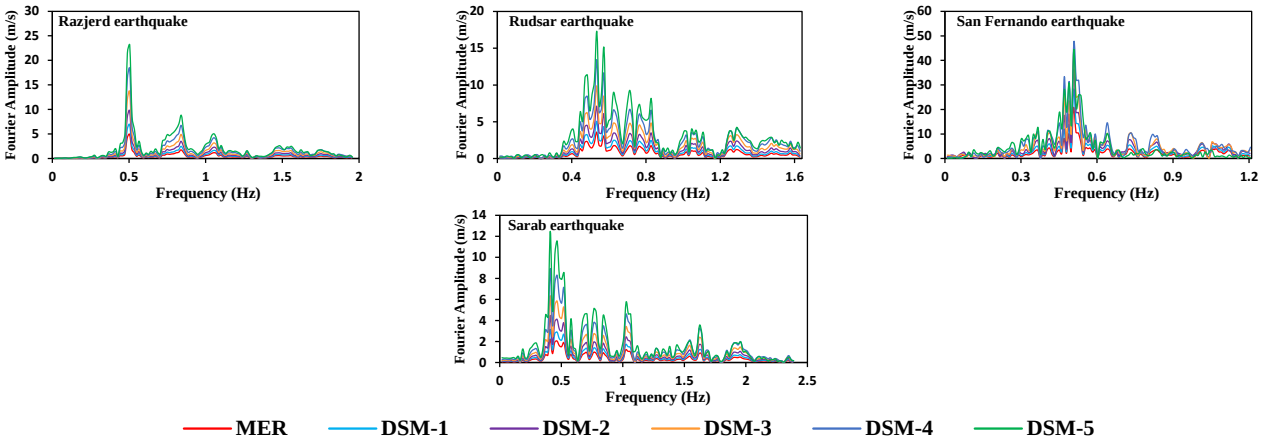

Fig. 12 Continued

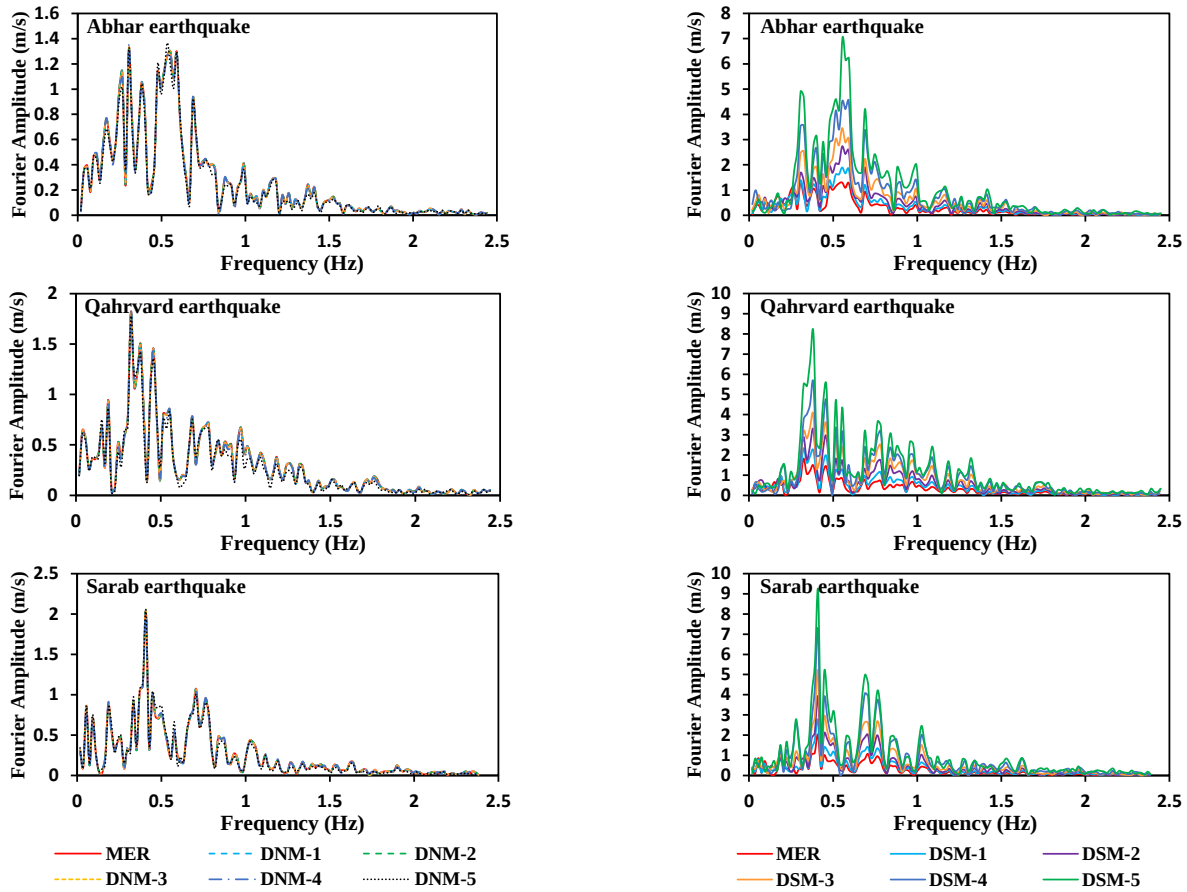

Fig. 13 Fourier amplitude spectrum at the dam crest (H=150 m) under MERs and decomposed records, DNM-based records (left column) and DSM-based records (right column)

2017, Javdanian and Lee 2019, Javdanian 2019) of acceleration response spectra was calculated to evaluate the accuracy of acceleration responses of the dam crest under main and wavelet-based decomposed earthquake records. Table 3 presents the values of RMSE for spectral acceleration responses of the crest of the 50 m high embankment dam under DNM- and DSM-based decomposed earthquake records.

For 16 earthquakes used in this study, the average RMSE of spectral acceleration responses of the embankment dam under 1st to 5th level records decomposed by DNM equals 0.0064, 0.0238, 0.0956, 0.3125 and 0.6819, respectively. The corresponding values for the earthquake records decomposed by DSM are 1.3014, 2.7587, 4.3319, 6.0953 and 7.5180, respectively. Comparing the accuracy of acceleration response spectra of earthquake records decomposed by de-noising and down-sampling methods indicates the higher accuracy of seismic response analysis of the dams under DNM-based records (Table 3).

Figs. 9 and 10 depict the ratio of maximum spectral acceleration (Sa_{max}) of the crest of the 50 m high embankment dam under main earthquake records and

decomposed records up to the 5th level to the maximum spectral acceleration under the main earthquake record ($Sa_{max,MER}$), (i.e., $Sa_{max}/Sa_{max,\ MER}$). In these figures, a decomposition level of 0 indicates an un-decomposed earthquake record (i.e., main earthquake record, MER).

Fig. 9 depicts $Sa_{max}/Sa_{max.MER}$ for DNM-based decomposed earthquakes. As clearly seen in this figure, $Sa_{max}/Sa_{max.MER}$ is approximately 1 up to the 3rd level and about unity in the 4th level, $(Sa_{max,DNM-1,2,3,4}/Sa_{max,MER})\approx 1$. Although the maximum acceleration spectrum under DNM-based decomposed records is almost unity at the 5th level ($Sa_{max,DNM-5}/Sa_{max,MER}$), the results indicate the lower accuracy of dynamic analyses under DNM-5 records in comparison with main earthquake records (Fig. 9).

Fig. 10 shows $Sa_{max}/Sa_{max.MER}$ for acceleration response spectra of the crest of the 50 m high embankment dam under main earthquakes (Table 1) and DSM-based decomposed records. As depicted in this figure, $Sa_{max}/Sa_{max.MER}$ is approximately 1 up to the 2nd level ($Sa_{max,DSM-1,2}/Sa_{max,MER}\approx 1$) and greater than unity from the 3rd to 5th levels ($Sa_{max,DSM-3,4,5}/Sa_{max,MER} > 1$). Comparing $Sa_{max}/Sa_{max,MER}$ for the de-noising and down-sampling methods indicates that main earthquake records can be replaced by DNM-based and DSM-based decomposed earthquake records respectively up to the 4th and 2nd levels for seismic response analysis of embankment dams.

5.3 Fourier amplitude spectrum

Fourier amplitude spectrum (FAS) of acceleration of the crest of the 50 m high dam under main earthquakes and those decomposed by DNM and DSM methods are shwn in Figs. 11 and 12, respectively. The Fourier amplitude spectrum indicates distribution of amplitude with frequency. This spectrum indicates the significance of frequencies existing in a signal. Fourier spectrum is able to well express the frequency content of earthquake records (Kramer 1996). As shown in Fig. 11, the FAS of acceleration of the dam crest under DNM-based records is consistent with responses under main record.

The FAS of acceleration of the embankment dam crest under DSM-based decomposed earthquake records has an acceptable accuracy up to the 2nd level, and the difference between the spectra increases at higher decomposition levels (Fig. 12).

Fig. 13 shows the FAS of acceleration of the crest of the 150 m high dam under earthquake records decomposed by de-noising and down-sampling methods. As seen in Figs. 11- 13, the frequency corresponding to the maximum FAS of the dam crest under main earthquake records is consistent with that under wavelet-based decomposed earthquake records. The results also indicate the higher accuracy of DNM- than DSM-based decomposed records in seismic response analysis of high embankment dams (Fig. 13).

Comparing the FAS obtained from dynamic analysis under decomposed and main earthquake records indicates that the frequency content is less affected in wavelet de-noising decomposition than wavelet down-sampling decomposition. Accordingly, DNM-based decomposed records are able to play the same role of main earthquake records in dynamic analysis of embankment dams.

6. Conclusions

This study intended (attempts) to assess the seismic behavior of embankment dams with clay core under wavelet-based decomposed ground motion records. Earthquake records were decomposed using de-noising method (DNM) and down-sampling method (DSM) up to five levels. Low and high frequencies of the main earthquake motion were separated into approximation and detail signals, respectively, by de-noising method (DNM).

The approximation signal was again decomposed to attain a new approximation wave. Beside separation of the original ground motion, the number of acceleration-time records is also halved in the down-sampling method (DSM). In both approaches, the earthquake decomposition process continues until the difference between the approximation waves and main earthquake record is not noticeable. Embankment dams with the height of 50 m and 150 m were seismically analyzed through finite element program of Plaxis.

Seismic analyses of dams were carried out under 16 main earthquake records and 160 wavelet-based decomposed records. Acceleration response, spectral acceleration, and Fourier amplitude spectrum at the crest of embankment dams under main and decomposed records at different levels were investigated.

The acceleration responses of the crest of dams under main and decomposed earthquake records were investigated and compared. Comparisons indicate that the records decomposed by de-noising and down-sampling methods have a reasonable accuracy respectively up to the 4th and 2nd levels in evaluating seismic response of dams. Comparison of spectral acceleration responses and Fourier amplitude spectra of the dam crest under main and decomposed earthquake records also confirm this conclusion. Therefore, the main records can be replaced by wavelet-based decomposed records in dynamic analysis of dams. For 16 earthquake records used in this study, the average RMSE of acceleration response spectra of the crest of the 50 m high embankment dam under the 4th and 5th levels earthquake records decomposed by DNM equals 0.3125 and 0.6819, respectively.

The RMSE parameter for the acceleration response spectrum under the 2nd and 3rd levels records decomposed by DSM equals 2.7587 and 4.3319, respectively. It is noteworthy that the frequency content of the main earthquake record (MER) is less affected by wavelet de-noising decomposition than wavelet down-sampling method.

The results of dynamic analyses indicate the higher accuracy of DNM-based decomposed earthquake records than DSM-based decomposed records in evaluating dynamic behavior of embankment dams. Accordingly, DNM-based records are able to play the same role of main earthquake records in dynamic analysis of embankment dams more effectively. Evaluating acceleration responses of the 50 m and 150 m high embankment dams under main and decomposed earthquake indicates a decrease in the horizontal acceleration response of the dam crest with increasing height of embankment dam.

According to the results of dynamic analyses, there is a

good consistency between the periods corresponding to maximum spectral acceleration (Sa_{max}) responses of embankment dam crest under main earthquake records and wavelet-based decomposed records. The same frequency corresponding to the maximum Fourier amplitude spectrum (FAS) of dam crest under main and decomposed records indicates high accuracy of wavelet-based decomposed earthquake records in evaluating the seismic behavior of embankment dams.

References

Aliberti, D., Cascone, E. and Biondi, G. (2016), "Seismic performance of the San Pietro dam", *Procedia Eng*. **158**, 362-367. https://doi.org/10.1016/j.proeng.2016.08.456.

Amorosi, A., Boldini, D. and Di Lernia, A. (2016), "Seismic ground response at Lotung: Hysteretic elasto-plastic-based 3D analyses", *Soil Dyn. Earthq. Eng.*, **85**, 44-61. https://doi.org/10.1016/j.soildyn.2016.03.001.

Andrianopoulos, K.I., Papadimitriou, A.G., Bouckovalas, G.D. and Karamitros, D.K. (2014), "Insight into the seismic response of earth dams with an emphasis on seismic coefficient estimation", *Comput. Geotech.*, **55**, 195-210. https://doi.org/10.1016/j.compgeo.2013.09.005.

Ansari, A., Noorzad, A. and Zare, M. (2007), "Application of wavelet multi-resolution analysis for correction of seismic acceleration records", *J. Geophys. Eng.*, **4**(4), 362-377. https://doi.org/10.1088/1742-2132/4/4/002.

Ansari, A., Noorzad, A., Zafarani, H. and Vahidifard, H. (2010), "Correction of highly noisy strong motion records using a modified wavelet de-noising method", *Soil Dyn. Earthq. Eng.*, **30**(11), 1168-1181. https://doi.org/10.1016/j.soildyn.2010.04.025.

Apaydin, N.M., Bas, S. and Harmandar, E. (2016), "Response of the Fatih Sultan Mehmet Suspension Bridge under spatially varying multi-point earthquake excitations", *Soil Dyn. Earthq. Eng.*, **84**, 44-54. https://doi.org/10.1016/j.soildyn.2016.01.018.

Banjade, T.P., Yu, S. and Ma, J. (2019), "Earthquake accelerogram denoising by wavelet-based variational mode decomposition", *J. Seismol.*, **23**(4), 649-663. https://doi.org/10.1007/s10950-019-09827-0.

Bas, S., Apaydin, N.M., Harmandar, E., and Catbas, N. (2018), "Multi-point earthquake response of the Bosphorus Bridge to site-specific ground motions", *Steel Compos. Struct.*, **26**(2), 197-211. https://doi.org/10.12989/scs.2018.26.2.197.

Bayraktar, A. and Kartal, M.E. (2010), "Linear and nonlinear response of concrete slab on CFR dam during earthquake" *Soil Dyn. Earthq. Eng.*, **30**(10), 990-1003. https://doi.org/10.1016/j.soildyn.2010.04.010.

Brinkgreve, R.B.J. (2002), Plaxis 2D: finite element code for soil and rock analyses, Version 8, Balkema Publisher, The Netherlands.

Cascone, E. and Rampello, S. (2003), "Decoupled seismic analysis of an earth dam", *Soil Dyn. Earthq. Eng.*, **23**(5), 349-365. https://doi.org/10.1016/S0267-7261(03)00035-6.

Castelli, F., Lentini, V. and Trifaro, C.A. (2016), "1D seismic analysis of earth dams: the example of the Lentini site", *Procedia Eng.*, **158**, 356-361. https://doi.org/10.1016/j.proeng.2016.08.455.

Chakraborty, S., Das, J.T., Puppala, A.J. and Banerjee, A. (2019), "Natural frequency of earthen dams at different induced strain levels", *Eng. Geol.*, **248**, 330-345. https://doi.org/10.1016/j.enggeo.2018.12.008.

Charatpangoon, B., Kiyono, J., Furukawa, A. and Hansapinyo, C. (2014), "Dynamic analysis of earth dam damaged by the 2011 off the Pacific Coast of Tohoku earthquake", *Soil Dyn. Earthq. Eng.*, **64**, 50-62. https://doi.org/10.1016/j.soildyn.2014.05.002.

Chen, M. and Harichandran, R.S. (2001), "Response of an earth dam to spatially varying earthquake ground motion", *J. Eng. Mech.*, **127**(9), 932-939. https://doi.org/10.1061/(ASCE)0733-9399(2001)127:9(932).

Chen, S.S., Fu, Z.Z., Wei, K.M. and Han, H.Q. (2016), "Seismic responses of high concrete face rockfill dams: A case study", *Water Sci. Eng.*, **9**(3), 195-204. https://doi.org/10.1016/j.wse.2016.09.002.

Crochiere, R.E. (1981), "Digital signal processor: Sub-band coding", *Bell Syst. Tech. J.*, **60**(7), 1633-1653. https://doi.org/10.1002/j.1538-7305.1981.tb00288.x.

Daubechies, I. (1990), "The wavelet transform, time-frequency localization and signal analysis", *IEEE T. Inf. Theor.*, **36**(5), 961-1005. https://doi.org/10.1109/18.57199.

Davoodi, M., Jafari, M.K. and Hadiani, N. (2013a), "Seismic response of embankment dams under near-fault and far-field ground motion excitation", *Eng. Geol.*, **158**, 66-76. https://doi.org/10.1016/j.enggeo.2013.02.008.

Davoodi, M., Jafari, M.K. and Sadrolddini, S.M.A. (2013b), "Effect of multi-support excitation on seismic response of embankment dams", *Int. J. Civ. Eng.*, **11**(1), 19-28.

Ding, X.M., Liu, H.L., Yu, T. and Kong, G.Q. (2013), "Nonlinear finite element analysis of effect of seismic waves on dynamic response of Shiziping dam", *J. Central South Univ.*, **20**(8), 2323-2332. https://doi.org/10.1007/s11771-013-1740-3.

Ebrahimian, B. (2011), "Numerical analysis of nonlinear dynamic behavior of earth dams", *Front. Archit. Civ. Eng. China*, **5**(1), 24-40. https://doi.org/10.1007/s11709-010-0082-6.

Elgamal, A.W.M., Scott, R.F., Succarieh, M.F. and Yan, L. (1990), "La Villita dam response during five earthquakes including permanent deformation", *J. Geotech. Eng.*, **116**(10), 1443-1462. https://doi.org/10.1061/(ASCE)0733-9410(1990)116:10(1443).

Farge, M. (1992). Wavelet transforms and their applications to turbulence. *Ann. Rev. Fluid Mech.*, **24**(1), 395-458. https://doi.org/10.1146/annurev.fl.24.010192.002143.

Feng, Z., Tsai, P.H. and Li, J.N. (2010), "Numerical earthquake response analysis of the Liyutan earth dam in Taiwan", *Nat. Hazards Earth Syst.*, **10**(6), 1269-1280. https://doi.org/10.5194/nhess-10-1269-2010.

Ghodrati Amiri, G., Rad, A.A. and Hazaveh, N.K. (2014), "Wavelet-based method for generating nonstationary artificial pulse-like near-fault ground motions", *Comput-Aided Civ. Inf. Eng.*, **29**(10), 758-770. https://doi.org/10.1111/mice.12110.

Haigh, S.K., Teymur, B., Madabhushi, S.P.G. and Newland, D.E. (2002), "Applications of wavelet analysis to the investigation of the dynamic behaviour of geotechnical structures", *Soil Dyn. Earthq. Eng.*, **22**(9-12), 995-1005. https://doi.org/10.1016/S0267-7261(02)00124-0.

Heidari, A., Pahlavan Sadegh, S. and Raeisi, J. (2019), "Investigating the effect of soil type on non-linear response spectrum using wavelet theory", *Int. J. Civ. Eng.*, **17**(12), 1909-1918. https://doi.org/10.1007/s40999-019-00394-6.

Holschneider, M. (1995), *Wavelets: An Analysis Tool*, Oxford Science Publications, Oxford.

Hu, H. and Huang, Y. (2019), "A dynamic reliability approach to seismic vulnerability analysis of earth dams", *Geomech. Eng.*, **18**(6), 661-668. https://doi.org/10.12989/gae.2019.18.6.661.

Hwang, J.H., Wu, C.P. and Wang, S.C. (2007), "Seismic record analysis of the Liyutan earth dam", *Can. Geotech. J.*, **44**(11), 1351-1377. https://doi.org/10.1139/T07-062.

Jafarian, Y., Haddad, A. and Javdanian, H. (2015), "Comparing the shear stiffness of calcareous and silicate sands under dynamic and cyclic straining", *Proceedings of the 7th International Conference of Seismology and Earthquake Engineering (SEE7)*, Tehran, Iran, May.

Javdanian, H. (2019), "Evaluation of soil liquefaction potential

using energy approach: Experimental and statistical investigation", *Bull. Eng. Geol. Environ.*, **78**(3), 1697-1708. https://doi.org/10.1007/s10064-017-1201-6.

Javdanian, H. and Lee, S. (2019), "Evaluating unconfined compressive strength of cohesive soils stabilized with geopolymer: a computational intelligence approach", *Eng. Comput.*, **35**(1), 191-199. https://doi.org/10.1007/s00366-018-0592-8.

Javdanian, H. and Pradhan, B. (2019), "Assessment of earthquake-induced slope deformation of earth dams using soft computing techniques", *Landslides*, **16**(1), 91-103. https://doi.org/10.1007/s10346-018-1078-x.

Javdanian, H., Heidari, A. and Kamgar, R. (2017), "Energy-based estimation of soil liquefaction potential using GMDH algorithm", *Iran. J. Sci. Technol. Trans. Civ. Eng.*, **41**(3), 283-295. https://doi.org/10.1007/s40996-017-0061-4.

Javdanian, H., Shakarami, L. and Zarif Sanayei, H.R. (2018), "Modeling seismic settlement of earth dams due to earthquake loading", *Proceedings of the International Conference on New Findings of Civil, Architectural and Iran Building Industry*, Tehran, Iran, December.

Javdanian, H., Zarif Sanayei, H.R. and Shakarami, L. (2020), "A regression-based approach to the prediction of crest settlement of embankment dams under earthquake shaking", *Sci. Iran.* https://doi.org/10.24200/sci.2018.50483.1716.

Karabulut, M. and Genis, M. (2019), "Pseudo seismic and static stability analysis of the Torul Dam", *Geomech. Eng.*, **17**(2), 207-214. https://doi.org/10.12989/gae.2019.17.2.207.

Kaveh, A. and Mahdavi, V.R. (2016), "A new method for modification of ground motions using wavelet transform and enhanced colliding bodies optimization", *Appl. Soft Comput.*, **47**, 357-369. https://doi.org/10.1016/j.asoc.2016.06.021.

Kuhlemeyer, R.L. and Lysmer, J. (1973), "Finite element method accuracy for wave propagation problems", *J. Soil Mech. Found. Div.*, **99**, 421-427.

Lashgari, A., Jafarian, Y. and Haddad, A. (2018), "Predictive model for seismic sliding displacement of slopes based on a coupled stick-slip-rotation approach", *Eng. Geol.*, **244**, 25-40. https://doi.org/10.1016/j.enggeo.2018.07.017.

Moghaddam, A.B. and Bagheripour, M.H. (2014), "Optimization of ground response analysis using wavelet-based transfer function technique", *Geomech. Eng.*, **7**(2), 149-164. https://doi.org/10.12989/gae.2014.7.2.149.

Nasiri, F., Javdanian, H. and Heidari, A. (2019), "Behavior of earth dams due to downsampling-based records", *Proceedings of the 8th International Conference on Seismology and Earthquake Engineering (SEE8)*, Tehran, Iran, November.

Papadimitriou, A.G., Bouckovalas, G.D. and Andrianopoulos, K.I. (2014), "Methodology for estimating seismic coefficients for performance-based design of earthdams and tall embankments", *Soil Dyn. Earthq. Eng.*, **56**, 57-73. https://doi.org/10.1016/j.soildyn.2013.10.006.

Papalou, A. and Bielak, J. (2001), "Seismic elastic response of earth dams with canyon interaction", *J. Geotech. Geoenviron. Eng.*, **127**(5), 446-453. https://doi.org/10.1061/(ASCE)1090-0241(2001)127:5(446).

Papalou, A. and Bielak, J. (2004), "Nonlinear seismic response of earth dams with canyon interaction", *J. Geotech. Geoenviron. Eng.*, **130**(1), 103-110. https://doi.org/10.1061/(ASCE)1090-0241(2004)130:1(103).

Park, D.S. and Kim, N.R. (2017), "Safety evaluation of cored rockfill dams under high seismicity using dynamic centrifuge modeling", *Soil Dyn. Earthq. Eng.*, **97**, 345-363. https://doi.org/10.1016/j.soildyn.2017.03.020.

Pelecanos, L., Kontoe, S. and Zdravkovic, L. (2015), "A case study on the seismic performance of earth dams", *Geotechnique*, **65**(11), 923-935. https://doi.org/10.1680/jgeot.SIP.15.P.009.

Pelecanos, L., Kontoe, S. and Zdravkovic, L. (2018), "The effects of dam-reservoir interaction on the nonlinear seismic response of earth dams", *J. Earthq. Eng.*, 1-23. https://doi.org/10.1080/13632469.2018.1453409.

Rampello, S., Cascone, E. and Grosso, N. (2009), "Evaluation of the seismic response of a homogeneous earth dam", *Soil Dyn. Earthq. Eng.*, **29**(5), 782-798. https://doi.org/10.1016/j.soildyn.2008.08.006.

Rioul, O. and Vetterli, M. (1991), "Wavelets and signal processing", *IEEE Signal Process. Mag.*, **8**(4), 14-38. https://doi.org/10.1109/79.91217.

Russo, A.D., Sica, S., Del Gaudio, S., De Matteis, R. and Zollo, A. (2017), "Near-source effects on the ground motion occurred at the Conza Dam site (Italy) during the 1980 Irpinia earthquake", *Bull. Earthq. Eng.*, **15**(10), 4009-4037. https://doi.org/10.1007/s10518-017-0138-2.

Salajegheh, E. and Heidari, A. (2005a), "Optimum design of structures against earthquake by wavelet neural network and filter banks", *Earthq. Eng. Struct. Dyn.*, **34**(1), 67-82. https://doi.org/10.1002/eqe.417.

Salajegheh, E. and Heidari, A. (2005b), "Time history dynamic analysis of structures using filter banks and wavelet transforms", *Comput. Struct.*, **83**(1), 53-68. https://doi.org/10.1016/j.compstruc.2004.08.008.

Salajegheh, E., Heidari, A. and Saryazdi, S. (2005), "Optimum design of structures against earthquake by discrete wavelet transform", *Int. J. Numer. Meth. Eng.*, **62**(15), 2178-2192. https://doi.org/10.1002/nme.1279.

Shakarami, L., Javdanian, H., Zarif Sanayei, H.R. and Shams, G. (2019), "Numerical investigation of seismically induced crest settlement of earth dams", *Model. Earth Syst. Environ.*, **5**(4), 1231-1238. https://doi.org/10.1007/s40808-019-00624-9.

Sharafi, H. and Maleki, Y.S. (2019), "Evaluation of hazardous effects of near-fault earthquakes on earth dams by using EL and TNL numerical methods (case studies: Gheshlagh Oleya and Jamishan dams)", *Nat. Hazards*, **98**(2), 451-484. https://doi.org/10.1007/s11069-019-03702-4.

Smyrou, E., Bal, I.E., Tasiopoulou, P. and Gazetas, G. (2016), "Wavelet analysis for relating soil amplification and liquefaction effects with seismic performance of precast structures", *Earthq. Eng. Struct. Dyn.*, **45**(7), 1169-1183. https://doi.org/10.1002/eqe.2701.

Sonmezer, Y.B. and Celiker, M. (2020), "Determination of seismic hazard and soil response of a critical region in Turkey considering far field and near field earthquake effect", *Geomech. Eng.*, **20**(2), 131-146. https://doi.org/10.12989/gae.2020.20.2.131.

Sonmezer, Y.B., Bas, S., Isik, N.S. and Akbas, S.O. (2018), "Linear and nonlinear site response analyses to determine dynamic soil properties of Kirikkale", *Geomech. Eng.*, **16**(4), 435-448. https://doi.org/10.12989/gae.2018.16.4.435.

Sonmezer, Y.B., Celiker, M. and Bas, S. (2019), "An investigation on the evaluation of dynamic soil characteristics of the Elazig City through the 1-D equivalent linear site-response analysis", *Bull. Eng. Geol. Environ.*, **78**(7), 4689-4712. https://doi.org/10.1007/s10064-018-01450-6.

Strang, G. and Nguyen, T. (1996), *Wavelets and Filter Banks*, Wellesley-Cambridge Press, 514.

Suarez, L.E. and Montejo, L.A. (2007), "Applications of the wavelet transform in the generation and analysis of spectrum-compatible records", *Struct. Eng. Mech.*, **27**(2), 173-197. https://doi.org/10.12989/sem.2007.27.2.173.

Terzi, N.U. and Selcuk, M.E. (2015), "Nonlinear dynamic behavior of pamukcay earthfill dam", *Geomech. Eng.*, **9**(1), 83-100. https://doi.org/10.12989/gae.2015.9.1.083.

To, A.C., Moore, J.R. and Glaser, S.D. (2009), "Wavelet denoising

techniques with applications to experimental geophysical data", *Signal Process*., **89**(2), 144-160. https://doi.org/10.1016/j.sigpro.2008.07.023.

Uddin, N. (1999), "A dynamic analysis procedure for concrete-faced rockfill dams subjected to strong seismic excitation", *Comput. Struct*., **72**(1-3), 409-421. https://doi.org/10.1016/S0045-7949(99)00011-5.

Wang, J., Yang, G., Liu, H., Nimbalkar, S.S., Tang, X. and Xiao, Y. (2017), "Seismic response of concrete-rockfill combination dam using large-scale shaking table tests", *Soil Dyn. Earthq. Eng*., **99**, 9-19. https://doi.org/10.1016/j.soildyn.2017.04.015.

Xu, B., Zou, D., Kong, X., Hu, Z. and Zhou, Y. (2015), "Dynamic damage evaluation on the slabs of the concrete faced rockfill dam with the plastic-damage model", *Comput. Geotech*., **65**, 258-265. https://doi.org/10.1016/j.compgeo.2015.01.003.

Yao, Y., Wang, R., Liu, T. and Zhang, J.M. (2019), "Seismic response of high concrete face rockfill dams subjected to non-uniform input motion", *Acta Geotech*., **14**(1), 83-100. https://doi.org/10.1007/s11440-018-0632-y.

Zou, D., Xu, B., Kong, X., Liu, H. and Zhou, Y. (2013), "Numerical simulation of the seismic response of the Zipingpu concrete face rockfill dam during the Wenchuan earthquake based on a generalized plasticity model", *Comput. Geotech*., **49**, 111-122. https://doi.org/10.1016/j.compgeo.2012.10.010.

CC